AIAA AVIATION Forum
August 2-6, 2021, VIRTUAL EVENT
AIAA AVIATION 2021 FORUM

10.2514/6.2021-2907

Focused Laser Differential Interferometry Transfer Functions for Complex Density Disturbance Fields

A. Hameed* and N. J. Parziale†
Stevens Institute of Technology, Hoboken, NJ 07030, USA

In this paper, we re-derive some known transfer functions to reduce FLDI data. We derive additional transfer functions intended to model increasingly complex disturbance fields that account for disturbances not only in the streamwise direction, x, but the two spanwise directions, y and z, as well. Performing experiments with a round, turbulent jet, we show that increasing the complexity of the transfer function has merit with some qualifications.

I. Introduction

Focused laser differential interferometry (FLDI) is a novel nonparticle-based optical flow diagnostic technique pioneered by Smeets[1–6] and Smeets and George[7] in the 1970s. Smeets and George demonstrated the use of FLDI for measurements of a density profile within a shock front, unsteady boundary layers, and, amongst other things, developed an eight beam pair FLDI set-up to examine the flow field around a blunt cone. From the 1980s to the 2000s, other researchers have used laser differential interferometry (LDI) to make measurements in high-speed flows.[8–13] More recently, Parziale et al.[14–20] used the FLDI technique to characterize facility disturbance level and boundary-layer instability and transition in the Caltech T5 reflected-shock tunnel. Since that time researchers have made additional advancements including making reliable convective velocity measurements between two closely spaced FLDI probe volumes,[21–28] facility disturbance-level characterization[29–31], and novel beam shaping techniques for application in hard-to-access flows.[32–36] Additionally, researchers have devised controlled problems[37–39] to test the data-reduction strategies by Fulghum[40], Settles and Fulghum[41], and Schmidt and Shepherd[42].

Transfer functions are used to relate the measured FLDI response to that of an ideal FLDI instrument. For an FLDI system, the changing size of the beam along the beam propagation axis and the different points of the disturbance field that are being probed need to be incorporated into the transfer function. In this paper, we propose a method to formulate transfer functions for the FLDI instrument from first principles, present transfer functions for disturbance fields of increasing complexity, and apply these transfer functions to the measured FLDI response as the instrument probes the exit flow of a free-jet.

II. Model of the FLDI and Relation to Voltage Output

In an FLDI system, two beams traverse closely-spaced paths (in this case, the z direction - see Fig. 1) and are mixed with a polarization optic and then registered at a photodetector. The voltage response, V, from the photodetector is the integrated intensity over the sensor face,

$$V = \bar{I}_D R_S R_L = R_S R_L \iint_{A_S} I_D(x, y)\, dA_S, \tag{1}$$

where $I_D(x, y)$, $\bar{I}_D$, R_S, R_L, and A_S are the intensity at the detector face, integrated intensity, the responsivity of the photodetector, the load resistance, and the sensor area, respectively. The intensity at photodetector face can be related to the phase change as

$$\bar{I}_D = \bar{I}_1 + \bar{I}_2 + 2\sqrt{\bar{I}_1 \bar{I}_2}\cos(\Delta\Phi), \tag{2}$$

where $\bar{I}_1$ and $\bar{I}_2$ are the integrated intensity of each FLDI beam. Assuming $\bar{I}_1 = \bar{I}_2 = \bar{I}_0/2$ and the instrument is shifted by $\pi/2$ to the middle of a fringe, this reduces Eq. 2 to

$$\bar{I}_D = \bar{I}_0 + \bar{I}_0 \sin(\Delta\Phi). \tag{3}$$

*Graduate Student, Mechanical Engineering, 1 Castle Point on Hudson, Hoboken, New Jersey, 07030.
†Associate Professor, Mechanical Engineering, Castle Point on Hudson, Hoboken, New Jersey, 07030, Senior AIAA Member.

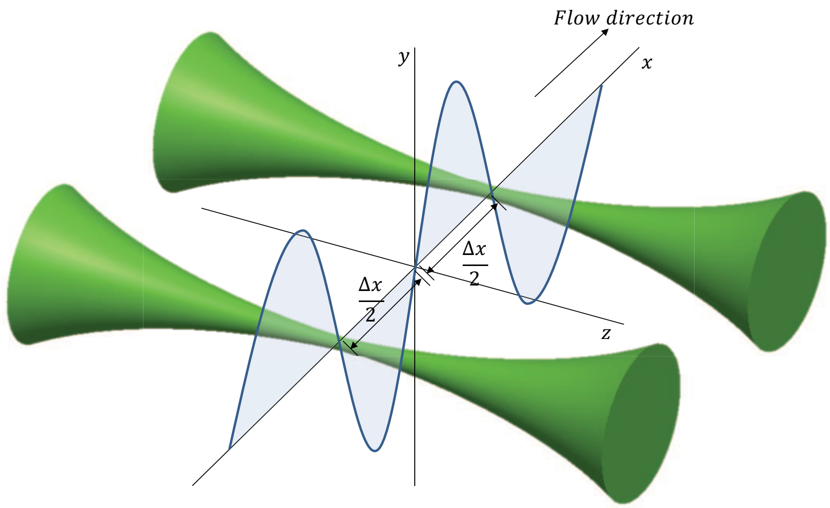

Fig. 1 Representation of FLDI beam pairs at spatial origin.

Equations 1 and 3 can be combined to relate the voltage to the phase change as

$$\Delta\Phi = \sin^{-1}\left(\frac{V_D - V_0}{V_0}\right). \tag{4}$$

Assuming that the beam propagation direction is in the z−direction, the phase-response of the FLDI is sensitive to optical-path-length ($OPL = \int n dz$) differences between the two beams at the detector as

$$\Delta\Phi = \frac{2\pi}{\lambda}\left(OPL_1 - OPL_2\right) = \frac{2\pi}{\lambda}\left(\int n(x,y,z)\,ds_1 - \int n(x,y,z)\,ds_2\right), \tag{5}$$

where $n(x, y, z)$ is the index of refraction of the disturbance field, λ is the wavelength of the laser, and s_1 and s_2 are the paths of the two FLDI beams. As such, to calculate the OPL of an FLDI beam that will be registered at a photodetector, we weight the local index of refraction by the local intensity. We write this as

$$OPL = \int n ds = \frac{1}{\iint_A I(x,y,z)\,dA}\iint_A \int_s I(x,y,z)n(x,y,z)\,dz\,dA. \tag{6}$$

That is, this model weighs more heavily those changes in index-of-refraction which occur at higher levels of intensity. This is because the phase change is related to the voltage (Eq. 4), and the voltage is linearly proportional to the beam intensity (Eq. 1). We assume a Gaussian beam with an intensity profile given by

$$I(x,y,z) = \frac{2}{w(z)^2\pi}\exp\left[\frac{-2(x^2+y^2)}{w(z)^2}\right], \tag{7}$$

where $w(z)$ is the $1/e^2$ radius of the beam varying along its propagation axis, z, and is given by

$$w(z) = \sqrt{w_0^2\left(1 + \left[\frac{\lambda z}{\pi w_0^2}\right]^2\right)}, \tag{8}$$

where, w_0 is the beam waist radius at the point of best focus. For a Gaussian beam, $\iint_{-\infty}^{\infty} I(x, y, z)\, dxdy = 1$ for any z. With these assumptions, we can write Eq. 5 as

$$\Delta\Phi = \frac{2\pi}{\lambda}\left[\iint_{-\infty}^{\infty}\int_s I\left(x - \frac{\Delta x}{2}, y, z\right)\ n(x, y, z)\, dz\, dx\, dy - \iint_{-\infty}^{\infty}\int_s I\left(x + \frac{\Delta x}{2}, y, z\right)\ n(x, y, z)\, dz\, dx\, dy\right]. \tag{9}$$

Here, we model the OPL difference by weighting the OPL of each beam with the beam intensity. Each FLDI beam is displaced from the origin by half the beam spacing, Δx, along the ordinate as $I\left(x \pm \frac{\Delta x}{2}, y, z\right)$, as in Fig. 1. The Gladstone-Dale relation is $n = K\rho + 1$, where K is the Gladstone-Dale constant and ρ is the local density. Plugging the Gladstone-Dale relation into Eq. 9 and dividing by the beam spacing yields

$$\begin{aligned}
\frac{\Delta\Phi}{\Delta x} =& \frac{2\pi K}{\Delta x\lambda}\left[\iint_{-\infty}^{\infty}\int_s I\left(x - \frac{\Delta x}{2}, y, z\right)\ \rho(x, y, z)\, dz\, dx\, dy - \iint_{-\infty}^{\infty}\int_s I\left(x + \frac{\Delta x}{2}, y, z\right)\ \rho(x, y, z)\, dz\, dx\, dy\right] \\
=& \frac{2\pi K}{\Delta x\lambda}\left[\iint_{-\infty}^{\infty}\int_s \left[I\left(x - \frac{\Delta x}{2}, y, z\right)\ \rho(x, y, z) - I\left(x + \frac{\Delta x}{2}, y, z\right)\ \rho(x, y, z)\right] dz\, dx\, dy\right] \\
=& \frac{2\pi K}{\Delta x\lambda}\left[\iint_{-\infty}^{\infty}\int_s \rho(x, y, z)\left[I\left(x - \frac{\Delta x}{2}, y, z\right)\ - I\left(x + \frac{\Delta x}{2}, y, z\right)\ \right] dz\, dx\, dy\right].
\end{aligned} \tag{10}$$

III. Relation of Discrete Phase Change to Differential Phase Change via Transfer Function

Ideally, an FLDI instrument would be able to measure differential, not discrete, changes in density, as the results may be more easily understood in frequency space. Following SS [42] and SF [41], we decrease the separation distance between the beams to a small value as

$$\frac{d\Phi}{dx} = \lim_{\Delta x \to 0}\frac{\Delta\Phi}{\Delta x} \tag{11}$$

Substituting Eq. 10 into equation Eq. 11 for $\frac{\Delta\Phi}{\Delta x}$, we get

$$\frac{d\Phi}{dx} = \lim_{\Delta x \to 0}\left[\frac{2\pi K}{\lambda\Delta x}\left[\iint_{-\infty}^{\infty}\int_s I\left(x - \frac{\Delta x}{2}, y, z\right)\ \rho(x, y, z) dzdxdy - \iint_{-\infty}^{\infty}\int_s I\left(x + \frac{\Delta x}{2}, y, z\right)\ \rho(x, y, z) dzdxdy\right]\right], \tag{12}$$

which reduces to

$$\frac{d\Phi}{dx} = \frac{2\pi K}{\lambda}\left[\iint_{-\infty}^{\infty} I(x, y, z)\int_s\left(\lim_{\Delta x \to 0}\frac{\rho_{x+\Delta x}(x, y, z) - \rho_x(x, y, z)}{\Delta x} dz\right) dz\, dx\, dy\right], \tag{13}$$

and, finally,

$$\frac{d\Phi}{dx} = \frac{2\pi K}{\lambda}\left[\iint_{-\infty}^{\infty} I(x, y, z)\int_s \frac{d\rho}{dx} dzdxdy\right] = \frac{2\pi K}{\lambda}\left[\iint_{-\infty}^{\infty} I(x, y, z) dxdy\int_s \frac{d\rho}{dx} dz\right]. \tag{14}$$

To further simplify, we note $\iint_{-\infty}^{\infty} I(x, y, z)\, dx\, dy = 1$, and, to eliminate the line integral in Eq. 14, we approximate the integration length to be equal to the characteristic length of the probe volume, L_P,

$$\frac{d\Phi}{dx} = \frac{2\pi K L_P}{\lambda}\frac{d\rho}{dx}. \tag{15}$$

Solving for $\frac{d\rho}{dx}$ and taking the Fourier transform of Eq. 15, we find

$$\mathcal{F}\left\{\frac{d\rho}{dx}\right\} = \frac{\lambda}{2\pi K L_P}\mathcal{F}\left\{\frac{d\Phi}{dx}\right\}. \tag{16}$$

We compute the Fourier transform of the density derivative using properties of the Fourier transform as

$$i\kappa_x\mathcal{F}\left\{\rho\right\} = \frac{\lambda}{2\pi K L}\mathcal{F}\left\{\frac{d\Phi}{dx}\right\}. \tag{17}$$

Now, we define a system transfer function of the FLDI instrument as the ratio of the measured instrument output at the detector to the expected instrument output of an ideal FLDI instrument,

$$H \equiv \frac{\left[\frac{\Delta\Phi}{\Delta x}\right]_{\text{measured}}}{\left[\frac{d\Phi}{dx}\right]_{\text{ideal}}}. \tag{18}$$

Using the definition of the transfer function, H, we relate the output of the instrument to the first derivative of the phase field. Solving for the derivative of the phase change in Eq. 18, we can make a substitution into Eq. 17 to obtain a relationship in frequency space between the measured fluctuations in phase to the actual density fluctuations as

$$\mathcal{F}\left\{\rho\right\} = \frac{1}{i\kappa_x}\frac{\lambda}{2\pi K L_P \Delta x}\mathcal{F}\left\{\frac{\Delta\Phi}{H}\right\}. \tag{19}$$

Now, we must model the disturbances to determine H.

IV. Derivation of Transfer Functions

In this section, we will re-derive transfer functions that were introduced by SS [42] and SF [41]. We will also introduce new transfer functions that attempt to capture more general flow disturbances.

To first re-derive the work in SS [42] and SF, we assume a sinusoidal disturbance in x, uniform in y, and infinitesimally thin in z at $z = 0$, of the form

$$\rho = \rho(x, y, z) = C sin(\kappa x + \phi_x)\delta(z), \tag{20}$$

where $\delta(z)$ is the Dirac delta. For simplicity, we set $C = 1$. Substituting the chosen form of the disturbance into Eq. 10 allows us to evaluate the line integral as

$$\begin{aligned}\frac{\Delta\Phi}{\Delta x} &= \frac{2\pi K}{\lambda\Delta x}\left[\iint_{-\infty}^{\infty}\sin(\kappa x + \phi_x)\left(I\left(x - \frac{\Delta x}{2}, y\right) - I\left(x + \frac{\Delta x}{2}, y\right)\right)dxdy\right] \\ &= \frac{2\pi K}{\lambda\Delta x}2\sin\left(\frac{\kappa\Delta x}{2}\right)\exp\left(-\frac{w^2\kappa^2}{8}\right)\cos(\phi_x).\end{aligned} \tag{21}$$

To evaluate the transfer function H for this disturbance, we must first evaluate $\frac{d\Phi}{dx}$, so rewrite Eq. 14 as

$$\frac{d\Phi}{dx} = \frac{2\pi K}{\lambda}\int_s \frac{d\rho}{dx}dz. \tag{22}$$

Plugging Eq. 20 into Eq. 22 results in

$$\frac{d\Phi}{dx} = \frac{2\pi K}{\lambda}\kappa\cos(\kappa x + \phi_x)\big|_{x=0} = \frac{2\pi K}{\lambda}\kappa\cos(\phi_x). \tag{23}$$

The ratio of Eq. 21 to Eq. 23 is the transfer function

$$H(\kappa) = \frac{2}{\kappa\Delta x}\sin\left(\frac{\kappa\Delta x}{2}\right)\exp\left(-\frac{w^2\kappa^2}{8}\right), \tag{24}$$

which is Eq. 18 in SS [42].

We next consider a disturbance field of the form (Fig. 2-left)

$$\rho(x, y, z) = \begin{cases}\sin(\kappa x + \phi_x) & -L \le z \le L \\ 0 & \text{otherwise.}\end{cases} \tag{25}$$

Substituting the chosen form of the disturbance into Eq. 10 yields

$$\begin{aligned}\frac{\Delta\Phi}{\Delta x} &= \frac{2\pi K}{\Delta x\lambda}\int_{-L}^{L}\iint_{-\infty}^{\infty}\sin(\kappa x + \phi_x)\left[I\left(x - \frac{\Delta x}{2}, y, z\right) - I\left(x + \frac{\Delta x}{2}, y, z\right)\right]\ dx\,dy\,dz \\ &= \frac{2\pi K}{\Delta x\lambda}2\sin\left(\frac{\kappa\Delta x}{2}\right)\cos(\phi_x)\int_{-L}^{L}\exp\left(-\frac{w(z)^2\kappa^2}{8}\right)\ dz \\ &= \frac{2\pi K}{\Delta x\lambda}2\sin\left(\frac{\kappa\Delta x}{2}\right)\cos(\phi_x)\frac{2\sqrt{2}\pi^{3/2}w_0}{\kappa\lambda}\exp\left(-\frac{w_0^2\kappa^2}{8}\right)\text{erf}\left[\frac{L\kappa\lambda}{2\sqrt{2}\pi w_0}\right].\end{aligned} \tag{26}$$

Plugging Eq. 25 into Eq. 22 results in

$$\frac{d\Phi}{dx} = \frac{2\pi K}{\lambda}\int_{-L}^{L}\frac{d\rho}{dx}dz = \frac{2\pi K}{\lambda}2L\kappa\cos(\kappa x+\phi_x)\big|_{x=0} = \frac{2\pi K}{\lambda}2L\kappa\cos(\phi_x). \tag{27}$$

The ratio of Eq. 26 to Eq. 27 is the transfer function

$$H = \frac{2\sqrt{2}\pi^{3/2}w_0}{\kappa^2\lambda\Delta x L}\sin\left(\frac{\kappa\Delta x}{2}\right)\exp\left(-\frac{w_0^2\kappa^2}{8}\right)\operatorname{erf}\left[\frac{L\kappa\lambda}{2\sqrt{2}\pi w_0}\right], \tag{28}$$

which is similar to a combination of Eqs. 16 and 17 in SS. Eq. 28 was intended to be used as a transfer function that would account for disturbances within a wind tunnel which had walls from $-L$ to L. However, assuming a disturbance has the structure of Eq. 27 may not be the best representation of a real flow field as L becomes large realtive to $1/\kappa$.

We will now introduce disturbances of increasingly complex form. First, let there be disturbances in x and y as,

$$\rho = \rho(x,y,z) = \sin(\kappa x+\phi_x)\sin(\kappa y+\phi_y)\delta(z). \tag{29}$$

Substituting the chosen form of the disturbance into Eq. 10 yields

$$\begin{aligned}\frac{\Delta\Phi}{\Delta x} &= \frac{2\pi K}{\Delta x\lambda}\iint_{-\infty}^{\infty}\sin(\kappa x+\phi_x)\sin(\kappa y+\phi_x)\left[I\left(x-\frac{\Delta x}{2},y,z\right)-I\left(x+\frac{\Delta x}{2},y,z\right)\right]\;dx\,dy\\ &= \frac{2\pi K}{\Delta x\lambda}2\sin\left(\frac{\kappa\Delta x}{2}\right)\exp\left(-\frac{w^2\kappa^2}{4}\right)\cos(\phi_x)\sin(\phi_y).\end{aligned} \tag{30}$$

The ratio of Eq. 30 to Eq. 23 is the transfer function

$$H(\kappa) = \frac{2}{\kappa\Delta x}\sin\left(\frac{\kappa\Delta x}{2}\right)\exp\left(-\frac{w^2\kappa^2}{4}\right), \tag{31}$$

where we are assuming $\phi_y = \pi/2$ and we justify using Eq. 23 as the denominator in the transfer function as we are only interested in the forming the spectrum from streamwise disturbances (x direction). That is, Eq. 31 accounts for the contribution of disturbances in y to the measurement of streamwise disturbances.

We next consider a disturbance field of the form (Fig. 2-right)

$$\rho(x,y,z) = \begin{cases}\sin(\kappa x+\phi_x)\sin(\kappa y+\phi_y) & -L\le z\le L\\ 0 & \text{otherwise,}\end{cases} \tag{32}$$

which following the above process yields

$$\begin{aligned}\frac{\Delta\Phi}{\Delta x} &= \frac{2\pi K}{\Delta x\lambda}\int_{-L}^{L}\iint_{-\infty}^{\infty}\sin(\kappa x+\phi_x)\sin(\kappa y+\phi_y)\left[I\left(x-\frac{\Delta x}{2},y,z\right)-I\left(x+\frac{\Delta x}{2},y,z\right)\right]\;dx\,dy\,dz\\ &= \frac{2\pi K}{\Delta x\lambda}2\sin\left(\frac{\kappa\Delta x}{2}\right)\cos(\phi_x)\sin(\phi_y)\int_{-L}^{L}\exp\left(-\frac{w(z)^2\kappa^2}{4}\right)\;dz\\ &= \frac{2\pi K}{\Delta x\lambda}2\sin\left(\frac{\kappa\Delta x}{2}\right)\cos(\phi_x)\sin(\phi_y)\frac{2\pi^{3/2}w_0}{\kappa\lambda}\exp\left(-\frac{w_0^2\kappa^2}{4}\right)\operatorname{erf}\left[\frac{L\kappa\lambda}{2\pi w_0}\right],\end{aligned} \tag{33}$$

which can be used with Eq. 23 to find

$$H(\kappa) = \frac{2\pi^{3/2}w_0}{\kappa^2\lambda\Delta x L}\sin\left(\frac{\kappa\Delta x}{2}\right)\exp\left(-\frac{w_0^2\kappa^2}{4}\right)\operatorname{erf}\left[\frac{L\kappa\lambda}{2\pi w_0}\right]. \tag{34}$$

Finally, we consider a disturbance field of the form

$$\rho(x,y,z) = \begin{cases}\sin(\kappa x+\phi_x)\sin(\kappa y+\phi_y)\sin(\kappa z+\phi_z) & -L\le z\le L\\ 0 & \text{otherwise.}\end{cases} \tag{35}$$

Plugging this disturbance into the phase change relation yields

$$
\begin{aligned}
\frac{\Delta\Phi}{\Delta x} &= \frac{2\pi K}{\Delta x \lambda}\int_{-L}^{L}\iint_{-\infty}^{\infty} \sin(\kappa x+\phi_x)\sin(\kappa y+\phi_y)\sin(\kappa z+\phi_z)\left[I\left(x-\frac{\Delta x}{2},y,z\right)-I\left(x+\frac{\Delta x}{2},y,z\right)\right]\ dx\,dy\,dz \\
&= \frac{2\pi K}{\Delta x\lambda}2\sin\left(\frac{\kappa\Delta x}{2}\right)\cos(\phi_x)\sin(\phi_y)\int_{-L}^{L}\sin(\kappa z+\phi_z)\exp\left(-\frac{w(z)^2\kappa^2}{4}\right)\,dz \\
&= \frac{2\pi K}{\Delta x\lambda}2\sin\left(\frac{\kappa\Delta x}{2}\right)\cos(\phi_x)\sin(\phi_y)\sin(\phi_z)\frac{i\pi^{3/2}w_0}{\kappa\lambda} \\
&\times\exp\left[-\frac{w_0^2}{4}\left(\kappa^2+\frac{4\pi^2}{\lambda^2}\right)\right]\left[\mathrm{erfi}\left[\frac{\pi w_0}{\lambda}-\frac{iL\kappa\lambda}{2\pi w_0}\right]-\mathrm{erfi}\left[\frac{\pi w_0}{\lambda}+\frac{iL\kappa\lambda}{2\pi w_0}\right]\right],
\end{aligned}
\tag{36}
$$

which can be used with Eq. 23 to find

$$
H(\kappa)=\frac{i\pi^{3/2}w_0}{\kappa^2\lambda\Delta x L}\exp\left[-\frac{w_0^2}{4}\left(\kappa^2+\frac{4\pi^2}{\lambda^2}\right)\right]\sin\left(\frac{\kappa\Delta x}{2}\right)\left[\mathrm{erfi}\left[\frac{\pi w_0}{\lambda}-\frac{iL\kappa\lambda}{2\pi w_0}\right]-\mathrm{erfi}\left[\frac{\pi w_0}{\lambda}+\frac{iL\kappa\lambda}{2\pi w_0}\right]\right]. \tag{37}
$$

The discrete domain ($-L \le z \le L$) over which the disturbance field exists makes the above transfer function difficult to evaluate. An attempt to simplify the computation is made using the identity $i \times \mathrm{erfi}(z) = \mathrm{erf}(i \times z)$. An equivalent transfer function is

$$
H(\kappa)=\frac{\pi^{3/2}w_0}{\kappa^2\lambda\Delta x L}\exp\left[-\frac{w_0^2}{4}\left(\kappa^2+\frac{4\pi^2}{\lambda^2}\right)\right]\sin\left(\frac{\kappa\Delta x}{2}\right)\left[\mathrm{erf}\left[\frac{i\pi w_0}{\lambda}+\frac{L\kappa\lambda}{2\pi w_0}\right]-\mathrm{erf}\left[\frac{i\pi w_0}{\lambda}-\frac{L\kappa\lambda}{2\pi w_0}\right]\right]. \tag{38}
$$

Further simplifying, we use the identity $\mathrm{erf}(-z) = -\mathrm{erf}(z)$ and $2\Re[\mathrm{erf}(x+i\times y)] = \mathrm{erf}(x+i\times y)+\mathrm{erf}(x-i\times y)$ with $x=\frac{L\kappa\lambda}{2\pi}$ and $y=\frac{\pi}{\lambda}$. Equation 38 becomes

$$
H(\kappa)=\frac{2\pi^{3/2}w_0}{\kappa^2\lambda\Delta x}\exp\left[-\frac{w_0^2}{4}\left(\kappa^2+\frac{4\pi^2}{\lambda^2}\right)\right]\sin\left(\frac{\kappa\Delta x}{2}\right)\left[2\Re\left[\mathrm{erf}\left[\frac{i\pi w_0}{\lambda}+\frac{L\kappa\lambda}{2\pi w_0}\right]\right]\right]. \tag{39}
$$

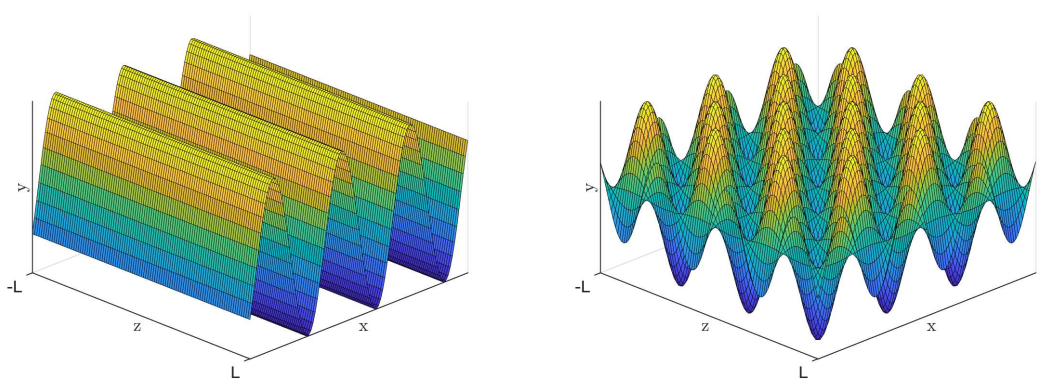

Fig. 2 Left: Density disturbance field of the form $\rho=\rho(x,y,z)=\sin(\kappa x)$ existing on the domain $-L\le z\le L$, with $\kappa=1$. Right: Density disturbance field of the form $\rho=\rho(x,y,z)=\sin(\kappa x+\phi_x)\sin(\kappa y+\phi_y)$ existing on the domain $-L\le z\le L$, with $\kappa=1$.

Alternatively, we can assume a sinusoidal disturbance in x, uniform in y, with a Gaussian width σ as

$$
\rho=\rho(x,y,z)=C\sin(\kappa x+\phi_x)\exp\left(\frac{-(z-z_0)^2}{\sigma^2}\right), \tag{40}
$$

where z_0 is the jet location. This disturbance may be useful to model the response of an FLDI to a turbulent jet of width σ. Plugging this form of the disturbance into the phase-change relation

$$\begin{aligned}\frac{\Delta\Phi}{\Delta x} &= \frac{2\pi K}{\Delta x\lambda}\int_{-\infty}^{\infty}\iint_{-\infty}^{\infty}\sin(\kappa x+\phi_x)\exp\left(\frac{-(z-z_0)^2}{\sigma^2}\right)\left[I\left(x-\frac{\Delta x}{2},y,z\right)-I\left(x+\frac{\Delta x}{2},y,z\right)\right]\,dx\,dy\,dz\\ &= \frac{2\pi K}{\Delta x\lambda}2\sin\left(\frac{\kappa\Delta x}{2}\right)\cos(\phi_x)\int_{-\infty}^{\infty}\exp\left(-\frac{w(z)^2\kappa^2}{8}\right)\exp\left(\frac{-(z-z_0)^2}{\sigma^2}\right)\,dz\\ &= \frac{2\pi K}{\Delta x\lambda}2\sin\left(\frac{\kappa\Delta x}{2}\right)\cos(\phi_x)\frac{2\pi^{3/2}w_0\sigma\exp\left[-\frac{1}{8}\kappa^2\left(w_0^2+\frac{8z_0^2\lambda^2}{8\pi^2w_0^2+\kappa^2\lambda^2\sigma^2}\right)\right]}{\sqrt{4\pi^2w_0^2+\frac{1}{2}\kappa^2\lambda^2\sigma^2}}\end{aligned} \tag{41}$$

To evaluate the transfer function H for this disturbance, we rewrite Eq. 14 as

$$\begin{aligned}\frac{d\Phi}{dx} &= \frac{2\pi K}{\lambda}\int_s\frac{d\rho}{dx}dz\\ &= \frac{2\pi K}{\lambda}\kappa\cos(\kappa x+\phi_x)\big|_{x=0}\int_{-\infty}^{\infty}\exp\left(\frac{-(z-z_0)^2}{\sigma^2}\right)\,dz\\ &= \frac{2\pi K}{\lambda}\kappa\cos(\phi_x)\sqrt{\pi}\sigma.\end{aligned} \tag{42}$$

The ratio of Eq. 40 to 42 is

$$H=\frac{4\pi w_0\sin\left(\frac{\kappa\Delta x}{2}\right)\exp\left[-\frac{1}{8}\kappa^2\left(w_0^2+\frac{8z_0^2\lambda^2}{8\pi^2w_0^2+\kappa^2\lambda^2\sigma^2}\right)\right]}{\kappa\Delta x\sqrt{4\pi^2w_0^2+\frac{1}{2}\kappa^2\lambda^2\sigma^2}}. \tag{43}$$

For an increasingly complex disturbance in x and y with a Gaussian width σ as

$$\rho=\rho(x,y,z)=C\sin(\kappa x+\phi_x)\sin(\kappa y+\phi_x)\exp\left(\frac{-(z-z_0)^2}{\sigma^2}\right), \tag{44}$$

yields

$$H=\frac{4\pi w_0\sin\left(\frac{\kappa\Delta x}{2}\right)\exp\left[-\frac{1}{4}\kappa^2\left(w_0^2+\frac{4z_0^2\lambda^2}{4\pi^2w_0^2+\kappa^2\lambda^2\sigma^2}\right)\right]}{\kappa\Delta x\sqrt{4\pi^2w_0^2+\frac{1}{2}\kappa^2\lambda^2\sigma^2}}, \tag{45}$$

following the above procedure. Finally, assuming a disturbance in of the form

$$\rho=\rho(x,y,z)=C\sin(\kappa x+\phi_x)\sin(\kappa y+\phi_x)\sin(\kappa z+\phi_x)\exp\left(\frac{-(z-z_0)^2}{\sigma^2}\right), \tag{46}$$

yields

$$H=\frac{4\pi\sin\left(\frac{\kappa\Delta x}{2}\right)\exp\left[-\frac{1}{4}w_0^2\kappa^2\left(1+\frac{4\pi^2\sigma^2}{4\pi^2w_0^2+\kappa^2\lambda^2\sigma^2}\right)\right]}{\kappa\Delta x\sigma\sqrt{\kappa^2\lambda^2/w_0^2+4\pi^2/\sigma^2}}, \tag{47}$$

where we've assumed $z_0=0$ for simplicity.

V. Facility and Experimental Setup

An FLDI setup was constructed to probe the exit of a sonic free-jet. To construct the FLDI setup, the linearly polarized laser beam produced by a Cobolt 05-01 series was expanded using a diverging lens. The expanding beam is then expanded using a diverging lens before being passed through two diffracting optics to generate a grid of beams 6 columns wide in the streamwise x-direction and 2 rows tall in the y-direction. The collection of beams is then circularly polarized by a quarter-wave plate before being split once more in the streamwise direction by a Wollaston prism.

Wollaston prisms of three different separation angles were used for these experiments: 2 arcminutes, 1 arcminute, and 0.5 arcminutes. The twelve orthogonally polarized beam pairs probe the jet exit flow. The beam pairs generated by the upbeam Wollaston prism are recombined by an equivalent Wollaston prism on the downbeam side. The interfence generated by the individual beams in the beam pairs traversing different optical path lenghts is manifested as fluctuations in intensity of the recombined beams and measured as changes in voltage by photodetectors. For these experiments, measurements from two of the twelve beam pairs are presented. A schematic of the setup is presented in Fig. 3.

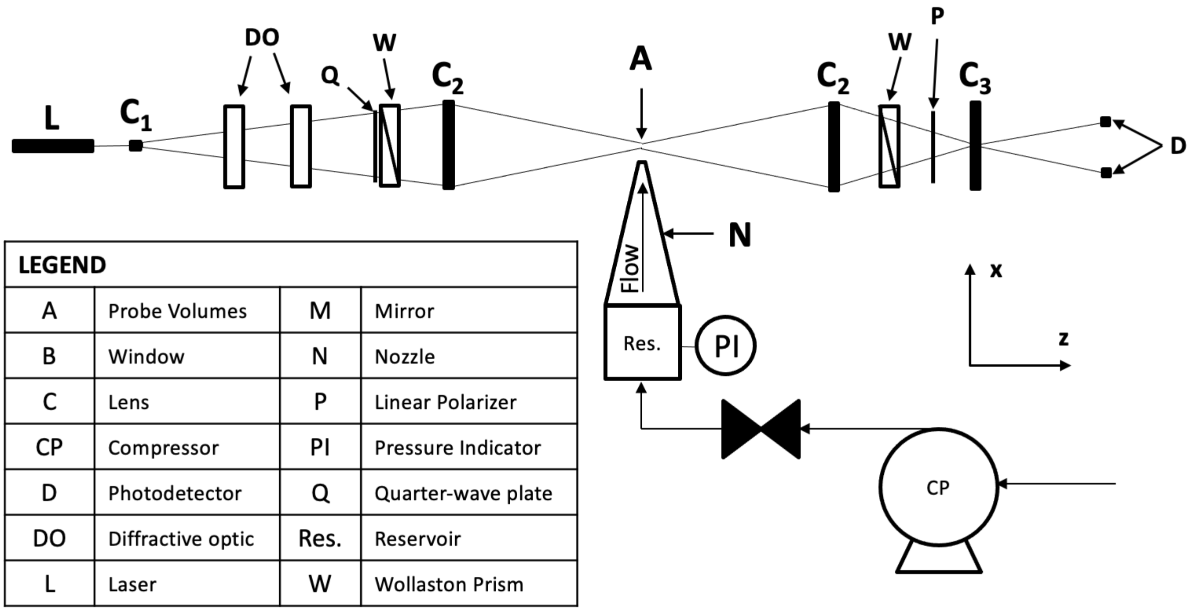

Fig. 3 Schematic of FLDI setup and components used to generate a turbulent jet. A combination of diffractive optics and Wollaston prisms were used to generate the beam pairs used to probe the flow at the exit of the jet.

Beam inter- and intraspacing generated using a 2 arcminute Wollaston prism is presented in Fig. 4. The beam interspacing was 1.639 mm, and the beam intraspacing was 262.53 μm. The beam interspacing did not change appreciably for the other Wollaston prisms used in this experimental campaign. The beam intraspacing using the 1 arcminute Wollaston prism was 85.20 μm and the intraspacing using the 0.5 arcminute Wollaston prism was 36.34 μm.

Fig. 4 FLDI beam pairs for an FLDI setup developed using diffractive optics and a 2 arcminute Wollaston prism pictured at the focus with an Ophir Spiricon LT665 beam profiler. The major tick marks are at 100 µm and the minor tick marks are at 50 µm.

The free-jet was generated in a laboratory setting. Compressed air was regulated to approximately 30 PSIG in the reservoir of a nozzle with an exit diameter of 0.147 inches. The nozzle was mounted on a platform that allowed for independent and precise adjustment in the x-, y-, and z-directions. For these experiments, the nozzle was positioned at the focus (z=0), 1.688 inches (x/D = 11.5) away from the FLDI beam pairs.

VI. Results

Results from the experiments are presented in this section. The dispersion relation for each experiment was first measured by correlation. It was determined following a procedure similar to the one described by Ceruzzi et al. [43]. An inverse tangent function was fitted to the individually calculated convective velocities to generate a continuous dispersion relation for all frequencies. The dispersion relations determined for the different beam intraspacings in each experiment are presented in Fig. 5.

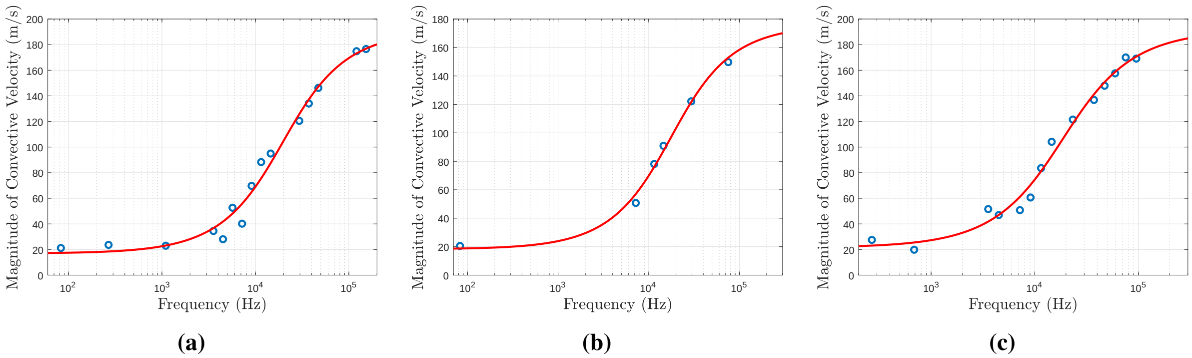

Fig. 5 Convective velocities and fit of dispersion relation for experiment with (a) 0.5 arcmimnute Wollaston prism, (b) 1 arcminute Wollaston prism, and (c) 2 arcminute Wollaston prism.

Using the dispersion relation, the transfer functions derived in the previous sections were determined for each experiment. Fig. 6 shows the transfer functions for the experiment using a 0.5 arcminute Wollaston prism. Note the similarity in shape and magnitude of the transfer functions for idealized disturbance fields. For these disturbance fields, the dimensional complexity of the disturbance does not seem to affect the transfer function. For disturbance fields occupying some physical space ($-L \leq z \leq L$ or σ), the transfer function tapers off depending on the width of the disturbance in z.

Due to their poor behavior, the transfer functions of three-dimensional disturbance fields (Eqs. 39 and 47) are not presented in this figure. We will continue to investigate these transfer functions and present our findings in future work. Their poor behavior most likely stems from the assumption that the disturbances are perfectly correlated along the z direction. The disturbances in x and y are also not perfectly correlated, as the simpler 1-D and 2-D transfer functions assume; however, the ratio of the disturbance length-scale to the integration length is less problematic. That is, $1/\kappa$ is closer in length scale to the beam waist $w(z)$ (for x and y integration) than it is L (for z integration).

Next, the power spectral densities (PSD) were computed for each experiment and corrected using the transfer functions to determine the expected response of an ideal FLDI instrument subjected to a disturbance field. Results for the experiment with a 0.5 arcminute Wollaston prism are presented in Fig. 7. As the complexity of the modeled disturbance field is increased to better align with the actual disturbance field (round turbulent jet), the PSD approaches the expected result. For an idealized disturbance infinitely small in space, of the form $\sin(\kappa x+\phi_x)\delta(z)$ or $\sin(\kappa x+\phi_x)\sin(\kappa y+\phi_y)\delta(z)$, an inertial subrange is not evident in the turbulent flowfield (Fig. 7a, c). It is not until the disturbance field more realistically occupies a physical space that the corrections yield an inertial subrange spanning approximately a decade, and a clear transition to the dissipation subrange at higher wavenumbers (Fig. 7b, d-f).

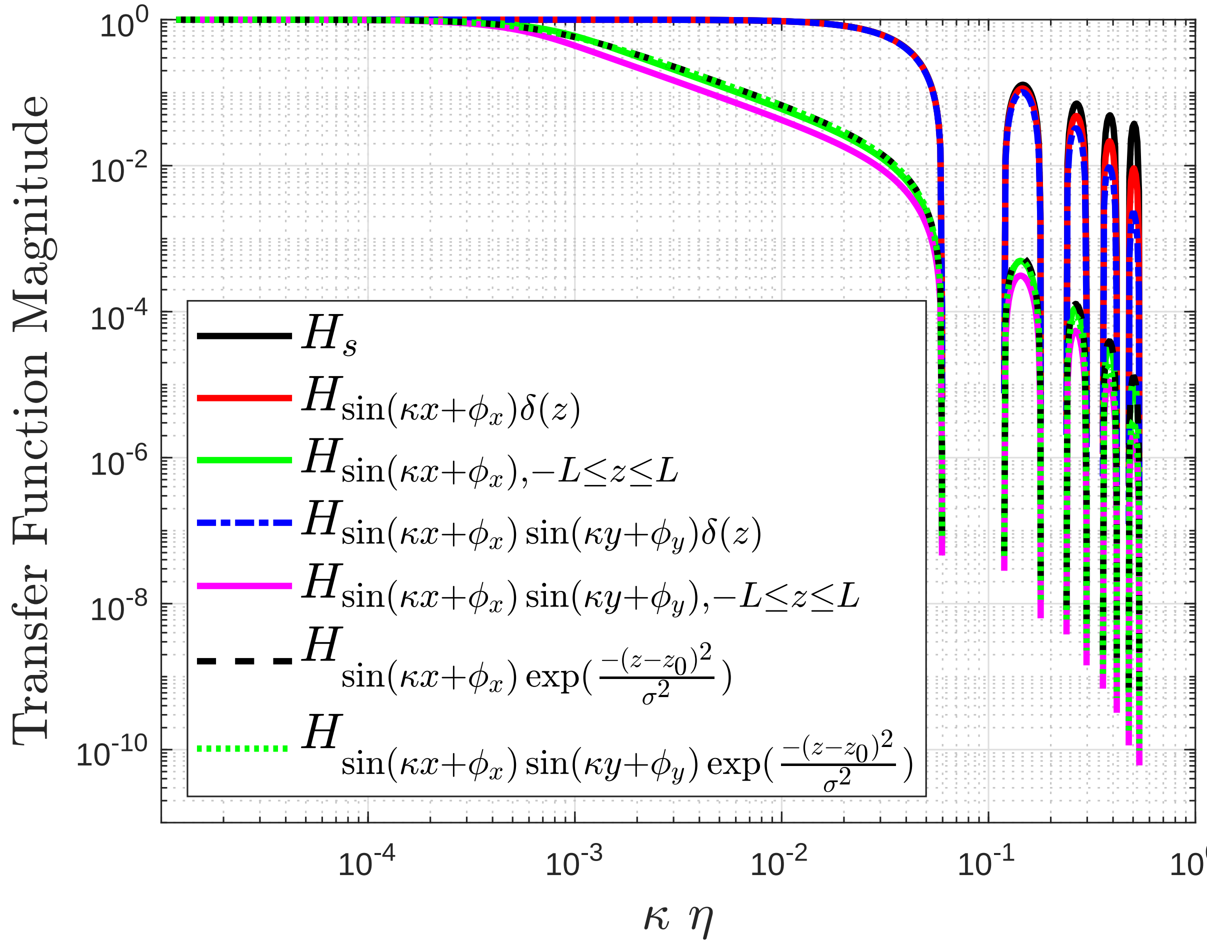

Fig. 6 Calculated transfer functions for experiment with 0.5 arcminute Wollaston prism. The transfer functions are presented with $\kappa\eta$ on the ordinate for consistency with the plotted power spectral densities. H_s is the transfer function that solely takes into account the changing beam size. The descriptors for the other transfer functions follow the disturbance fields modeled in previous sections.

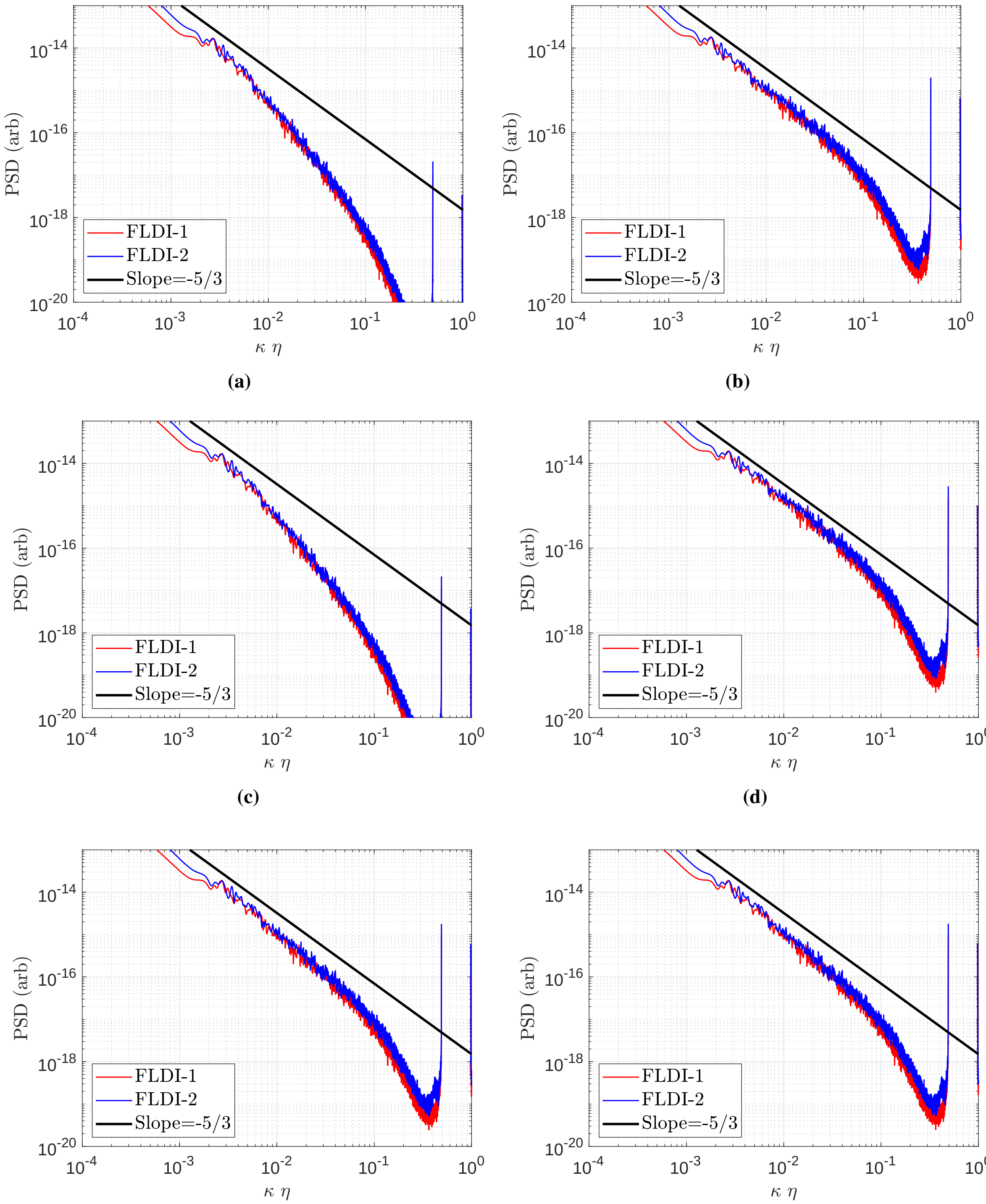

Fig. 7 PSDs for experiments performed with a 0.5 arcminute Wollaston prism to generate the beam intraspacing and a circular turbulent jet, corrected by transfer functions for disturbance fields of the form: (a) $\sin(\kappa x+\phi_x)\delta(z)$**, (b)** $\sin(\kappa x+\phi_x), -L \le z \le L$**, (c)** $\sin(\kappa x+\phi_x)\sin(\kappa y+\phi_y)\delta(z)$**, (d)** $\sin(\kappa x+\phi_x)\sin(\kappa y+\phi_y), -L \le z \le L$**, (e)** $\sin(\kappa x+\phi_x)\exp(\frac{-(z-z_0)^2}{\sigma^2})$**, and (f)** $\sin(\kappa x+\phi_x)\sin(\kappa y+\phi_y)\exp(\frac{-(z-z_0)^2}{\sigma^2})$**. Both FLDI beams in the d-FLDI setup are shown in each figure. The black line spanning each figure depicts a slope of** $-\frac{5}{3}$**, which is the expected slope of the inertial subrange in the Kolmogorov spectra.**

VII. Conclusion

In this paper, we re-derived some transfer functions to reduce FLDI data originally found in SS [42] and SF [41]. We derived additional transfer functions intended to account for increasingly complex disturbance fields that account for disturbances not only in the streamwise direction, x, but the two spanwise directions, y and z, as well. Performing experiments with a round, turbulent jet, we show that increasing the complexity of the transfer function has merit. The best results were had when modeling the field to include disturbances in x and y over a meaningful length scale in z, be it $2L$ or σ. However, including modeling the field to include disturbances in z resulted in a transfer function that did not yield meaningful results, most likely due to assumptions about how the disturbances are correlated along that integration direction.

Acknowledgments

Support for this work was provided by the Air Force Office of Scientific Research Grants FA9550-16-1-0262 and FA9550-18-1-0403; Ivett Leyva of AFOSR is the Program Manager for both grants. Additionally, there was support from Air Force Small Business Innovation Research contracts FA9101-17-P-0094 and FA2487-19-C-0013.

References

[1] Smeets, G., and George, A., "Gas Dynamic Investigations in a Shock Tube using a Highly Sensitive Interferometer," Translation of isl internal report 14/71, Original 1971, Translation 1996.

[2] Smeets, G., "Laser Interferometer for High Sensitivity Measurements on Transient Phase Objects," *IEEE Transactions on Aerospace and Electronic Systems*, Vol. AES-8, No. 2, 1972, pp. 186–190. https://doi.org/10.1109/TAES.1972.309488.

[3] Smeets, G., and George, A., "Anwendungen des Laser-Differentialinterferometers in der Gasdynamik," ISL - N 28/73, Also translated by Goetz, A.: ADA-307459, 1973.

[4] Smeets, G., "Laser-Interferometer mit grossen, fokussierten Lichtbündeln für lokale Messungen," ISL - N 11/73, 1973.

[5] Smeets, G., "Verwendung eines Laser-Differentialinterferometers zur Bestimmung lokaler Schwankungsgrössen sowie des mittleren Dichteprofils in cinem turbulenten Freistrahl," ISL - N 20/74, 1974.

[6] Smeets, G., "Flow Diagnostics by Laser Interferometry," *IEEE Transactions on Aerospace and Electronic Systems*, Vol. AES-13, No. 2, 1977, pp. 82–90. https://doi.org/10.1109/TAES.1977.308441.

[7] Smeets, G., and George, A., "Laser Differential Interferometer Applications in Gas Dynamics," Translation of ISL Internal Report 28/73, Original 1975, Translation 1996.

[8] Azzazy, M., Modarress, D., and Hoeft, T., "High sensitivity Density Fluctuation Detector," *Proceedings of SPIE Vol. 569 High Speed Photography, Videography, and Photonics I/I*, SPIE, San Diego, CA, 1985. https://doi.org/10.1117/12.949865.

[9] Azzazy, M., Modarress, D., and Trolinger, J. D., "Feasibility Study of Optical Boundary Layer Transition Detection Method," NASA-CR-178109, 1986.

[10] Azzazy, M., Modarress, D., and Hoeft, T., "High-sensitivity Density Fluctuation Detector," *Journal of Physics E: Scientific Instruments*, Vol. 20, No. 4, 1987, p. 428. https://doi.org/10.1088/0022-3735/20/4/017.

[11] O'Hare, J. E., "A Nonperturbing Boundary-Layer Transition Detector," *Proceedings of SPIE 0569, High Speed Photography, Videography, and Photonics III*, San Diego, California, 1985, pp. 58–63. https://doi.org/10.1117/12.949864.

[12] Collicott, S. H., Schneider, S. P., and Messersmith, N. L., "Review Of Optical Diagnostic Methods For Hypersonic Low-Noise Facilities," *Proceedings of 34th Aerospace Sciences Meeting and Exhibit*, AIAA-96-0851, Reno, NV, 1996. https://doi.org/10.2514/6.1996-851.

[13] Salyer, T. R., Collicott, S. H., and Schneider, S. P., "Feedback Stabilized Laser Differential Interferometry for Supersonic Blunt Body Experiments," *Proceedings of 38th Aerospace Sciences Meeting and Exhibit*, AIAA-2000-0416, Reno, Nevada, 2000. https://doi.org/10.2514/6.2000-416.

[14] Parziale, N. J., Shepherd, J. E., and Hornung, H. G., "Reflected Shock Tunnel Noise Measurement by Focused Differential Interferometry," *Proceedings of 42nd AIAA Fluid Dynamics Conference and Exhibit*, AIAA-2012-3261, New Orleans, Louisiana, 2012. https://doi.org/10.2514/6.2012-3261.

[15] Parziale, N. J., Jewell, J. S., Shepherd, J. E., and Hornung, H. G., "Optical Detection of Transitional Phenomena on Slender Bodies in Hypervelocity Flow," *Proceedings of RTO Specialists Meeting AVT-200/RSM-030 on Hypersonic Laminar-Turbulent Transition*, NATO, San Diego, California, 2012.

[16] Parziale, N. J., Shepherd, J. E., and Hornung, H. G., "Differential Interferometric Measurement of Instability at Two Points in a Hypervelocity Boundary Layer," *Proceedings of 51st AIAA Aerospace Sciences Meeting Including the New Horizons Forum and Aerospace Exposition*, AIAA-2013-0521, Grapevine, Texas, 2013. https://doi.org/10.2514/6.2013-521.

[17] Parziale, N. J., Shepherd, J. E., and Hornung, H. G., "Differential Interferometric Measurement of Instability in a Hypervelocity Boundary Layer," *AIAA Journal*, Vol. 51, No. 3, 2013, pp. 750–754. https://doi.org/10.2514/1.J052013.

[18] Parziale, N. J., "Slender-Body Hypervelocity Boundary-Layer Instability," Ph.D. thesis, California Institute of Technology, 2013.

[19] Parziale, N. J., Shepherd, J. E., and Hornung, H. G., "Free-stream density perturbations in a reflected-shock tunnel," *Experiments in Fluids*, Vol. 55, No. 2, 2014, p. 1665. https://doi.org/10.1007/s00348-014-1665-0.

[20] Parziale, N. J., Shepherd, J. E., and Hornung, H. G., "Observations of hypervelocity boundary-layer instability," *Journal of Fluid Mechanics*, Vol. 781, 2015, pp. 87–112. https://doi.org/10.1017/jfm.2015.489.

[21] Jewell, J. S., Parziale, N. J., Lam, K.-L., Hagen, B. J., and Kimmel, R. L., "Disturbance and Phase Speed Measurements for Shock Tubes and Hypersonic Boundary-Layer Instability," *Proceedings of 32nd AIAA Aerodynamic Measurement Technology and Ground Testing Conference*, AIAA-2016-3112, Washington, D. C., 2016. https://doi.org/10.2514/6.2016-3112.

[22] Jewell, J. S., Hameed, A., Parziale, N. J., and Gogineni, S. P., "Disturbance Speed Measurements in a Circular Jet via Double Focused Laser Differential Interferometry," *Proceedings of AIAA Scitech 2019*, AIAA-2019-2293, San Diego, California, 2019. https://doi.org/10.2514/6.2019-2293.

[23] Ceruzzi, A. P., and Cadou, C. P., "Simultaneous Velocity and Density Gradient Measurements using Two-Point Focused Laser Differential Interferometry," *Proceedings of AIAA Scitech 2019*, AIAA-2019-2295, San Diego, California, 2019. https://doi.org/10.2514/6.2019-2295.

[24] Ceruzzi, A. P., Callis, B., Weber, D., and Cadou, C. P., "Application of Focused Laser Differential Interferometry (FLDI) in a Supersonic Boundary Layer," *Proceedings of AIAA Scitech 2020*, AIAA-2020-1973, Orlando, Florida, 2020. https://doi.org/10.2514/6.2020-1973.

[25] Weisberger, J. M., Bathel, B. F., Herring, G. C., King, R. A., Chou, A., and Jones, S. B., "Focused Laser Differential Interferometry Measurements at NASA Langley 20-Inch Mach 6," *Proceedings of AIAA Aviation Forum*, AIAA-2019-2903, Dallas, Texas, 2019. https://doi.org/10.2514/6.2019-2903.

[26] Bathel, B. F., Weisberger, J. M., Herring, G. C., King, R. A., Jones, S. B., Kennedy, R. E., and Laurence, S. J., "Two-point, parallel-beam focused laser differential interferometry with a Nomarski prism," *Applied Optics*, Vol. 59, No. 2, 2020, pp. 244–252. https://doi.org/10.1364/AO.59.000244.

[27] Price, T. J., Gragston, M., Schmisseur, J. D., and Kreth, P. A., "Measurement of supersonic jet screech with focused laser differential interferometry," *Applied Optics*, Vol. 59, No. 28, 2020, pp. 8902–8908. https://doi.org/10.1364/AO.402011.

[28] Hameed, A., Parziale, N. J., Paquin, L., Butler, C., and Laurence, S. J., "Hypersonic Slender-Cone Boundary Layer Instability in the UMD HyperTERP Shock Tunnel," *Proceedings of AIAA SciTech 2020*, AIAA-2020-0362, Orlando, Florida, 2020. https://doi.org/10.2514/6.2020-0362.

[29] Harris, A. J., Kreth, P. A., Combs, C. S., and Schmisseur, J. D., "Laser Differential Interferometry and Schlieren as an Approach to Characterizing Freestream Disturbance Levels," *2018 AIAA Aerospace Sciences Meeting*, AIAA 2018-1100, Kissimmee, Florida, 2018. https://doi.org/10.2514/6.2018-1100.

[30] Lawson, J. M., and Austin, J. M., "Expansion Tube Freestream Disturbance Measurements using a Focused Laser Differential Interferometer," *Proceedings of AIAA Scitech 2020*, AIAA-2020-1064, Orlando, Florida, 2020. https://doi.org/10.2514/6.2020-1064.

[31] Birch, B., Buttsworth, D., and Zander, F., "Measurements of freestream density fluctuations in a hypersonic wind tunnel," *Experiments in Fluids*, Vol. 61, No. 7, 2020, pp. 1–13. https://doi.org/10.1007/s00348-020-02992-w.

[32] Hedlund, B., Houpt, A., Gordeyev, S., and Leonov, S., "Measurement of Flow Perturbation Spectra in Mach 4.5 Corner Separation Zone," *AIAA Journal*, Vol. 56, No. 7, 2018, pp. 2699–2711. https://doi.org/10.2514/1.J056576.

[33] Houpt, A. W., and Leonov, S. B., "Focused Laser Differential Interferometer for Supersonic Boundary Layer Measurements on Flat Plate Geometries," *Proceedings of the 2018 Plasmadynamics and Lasers Conference*, AIAA-2018-3434, Atlanta, Georgia, 2018. https://doi.org/10.2514/6.2018-3434.

[34] Houpt, A. W., and Leonov, S. B., "Focused and Cylindrical-Focused Laser Differential Interferometer Characterization of SBR-50 at Mach 2," *Proceedings of AIAA Aviation 2019*, AIAA-2019-3383, Dallas, Texas, 2019. https://doi.org/10.2514/6.2019-3383.

[35] Benitez, E. K., Jewell, J. S., and Schneider, S. P., "Focused Laser Differential Interferometry for Hypersonic Flow Instability Measurements with Contoured Tunnel Windows," *Proceedings of AIAA Scitech 2020*, AIAA-2020-1282, Orlando, Florida, 2020. https://doi.org/10.2514/6.2020-1282.

[36] Benitez, E. K., Esquieu, S., Jewell, J. S., and Schneider, S. P., "Instability Measurements on an Axisymmetric Separation Bubble at Mach 6," *Proceedings of AIAA Aviation 2020*, AIAA-2020-3072, Virtual Event, 2020. https://doi.org/10.2514/6.2020-3072.

[37] Ramprakash, A., McIntyre, T. J., Wheatley, V., and Mee, D. J., "Performance Analysis of FLDI Technique using Turbulent Jets," *Proceedings of the IX Australian Conference on Laser Diagnostics*, Adelaide, Australia, 2019.

[38] Lawson, J. M., Neet, M. C., Grossman, I. J., and Austin, J. M., "Characterization of a Focused Laser Differential Interferometer," *Proceedings of AIAA Scitech 2019*, AIAA-2019-2296, San Diego, California, 2019. https://doi.org/10.2514/6.2019-2296.

[39] Lawson, J. M., Neet, M. C., Grossman, I. J., and Austin, J. M., "Static and dynamic characterization of a focused laser differential interferometer," *Experiments in Fluids*, Vol. 61, No. 8, 2020, pp. 1–11. https://doi.org/10.1007/s00348-020-03013-6.

[40] Fulghum, M. R., "Turbulence measurements in high-speed wind tunnels using focusing laser differential interferometry," Ph.D. thesis, The Pennsylvania State University, 2014.

[41] Settles, G. S., and Fulghum, M. R., "The Focusing Laser Differential Interferometer, an Instrument for Localized Turbulence Measurements in Refractive Flows," *Journal of Fluids Engineering*, Vol. 138, No. 10, 2016, p. 101402. https://doi.org/10.1115/1.4033960.

[42] Schmidt, B. E., and Shepherd, J. E., "Analysis of focused laser differential interferometry," *Applied Optics*, Vol. 54, No. 28, 2015, pp. 8459–8472. https://doi.org/10.1364/AO.54.008459.

[43] Ceruzzi, A. P., Neisess, C., McManamen, B., and Cadou, C. P., "Investigation of Focused Laser Differential Interferometry (FLDI) Sensitivity Function," *Proceedings of AIAA Scitech 2021*, AIAA-2021-1299, Virtual Event, 2021. https://doi.org/10.2514/6.2021-1299.